

Microscopic scale of pair-breaking quantum phase transitions in superconducting films, nanowires and $\text{La}_{1.92}\text{Sr}_{0.08}\text{CuO}_4$

Andrey Rogachev¹ and Kevin Davenport¹

¹*Department of Physics and Astronomy, University of Utah, Salt Lake City 84093, USA*

(Dated: September 6, 2023)

The superconducting ground state in a large number of two-dimensional (2d) systems can be created and destroyed through quantum phase transitions (QPTs) driven by non-thermal parameters such as the carrier density or magnetic field [1–3]. The microscopic mechanism of QPTs has not been established in any 2d superconductor, in part due to an emergent scale-invariance near the critical point, which conceals the specific processes driving the transitions [4]. In this work, we find that the pair-breaking mechanism [5, 6] causing the suppression of the Cooper pair density gives a unifyingly consistent description of magnetic-field-driven QPTs in amorphous MoGe, Pb and TaN films, as well as in quasi-2d high-temperature superconductor $\text{La}_{1.92}\text{Sr}_{0.08}\text{CuO}_4$. This discovery was facilitated by the development of a novel theoretical approach, one which goes beyond the standard determination of critical exponents and allows for the extraction of a microscopic seeding length scale of the transitions. Remarkably, for the materials studied, and also for MoGe nanowires [7], this scale matches the superconducting coherence length. Further, this approach has been successfully applied to many other complex, non-superconducting systems [8, 9].

Two-dimensional (2d) superconductors constitute a large, rapidly growing class of materials ranging from thin films of conventional and high-temperature superconductors [10–14] to interface, surface, hybrid superconductors, and twisted bi-layer graphene [15–18]. Understanding QPTs in these systems is a challenging task [1]. Corresponding many-body 2d problems present a particularly hard case for the theory. The complexity of real materials exhibiting disorder and a tendency to form the spatially non-uniform state [1, 19–21], further complicates the field.

In proximity of a continuous QPT’s critical point, the quantum system becomes scale-invariant [4]. In apparent agreement with this prediction, the generic scaling behavior of conductivity has been observed in many 2d superconductors [22–25]. This behavior has been taken as the evidence for QPTs. However, the critical exponents obtained from the scaling analysis appear to vary unsystematically from system to system and don’t reveal the expected universality [1]. Moreover, the scaling behavior alone does not disclose the microscopic mechanism of QPTs [2] and, in fact, can be accidental [26].

There are several microscopic scenarios which can lead to a QPT in 2d superconductor. The most well-known, and most often used for comparison with experiments, is the dirty boson model [27]. It proposes that the transition occurs due to the delocalization of superconducting vortices and implies that the order parameter amplitude, the quantity which represents the density of the Cooper pairs, remains constant across the QPT and the superconductivity is destroyed entirely by phase fluctuations.

We have recently discovered, however, that all details of the magnetic-field-driven QPT in superconducting *nanowires* can be described by an alternative pair-breaking critical theory [6, 7]. Microscopically, the pair-breaking processes split Cooper pairs by acting on their orbital and spin parts. Cooper pair density goes to zero at the critical field, B_c , and the critical fluctuations in-

volve both amplitude and phase. The pair-breaking QPT is hidden by the contribution of normal electrons, which varies uncritically across the transition and accounts for about 90-95 percent of conductivity at the critical field.

Guided by the expectation that the magnetic-field-induced pair-breaking processes are similar in 1d and 2d [5], we have studied and analyzed the transitional regime in several superconducting 2d systems and discovered pronounced pair-breaking QPTs in amorphous MoGe, Pb and TaN films as well as in high-temperature superconductor $\text{La}_{1.92}\text{Sr}_{0.08}\text{CuO}_4$ (LSCO).

Pair-breaking quantum phase transition.

The details of the fabrication and measurements of films made of amorphous MoGe alloy are given in supplementary materials (SM). The data for the amorphous Pb films were traced from [28], for amorphous TaN from [29], and for LSCO from [30]. Magnetic field was oriented normal to the films and to CuO_2 layers in LSCO.

Figure 1(a) displays the temperature dependence of the resistance of film MG1 (composition $\text{Mo}_{50}\text{Ge}_{50}$, nominal thickness 2.5 nm, $T_c=1.2$ K) at the indicated magnetic fields. In the superconducting state, all curves display a roughly exponential variation with no sign of leveling to a finite value. This contrasts with the resistance saturation previously observed in MoGe films, as well as in many other systems, which was taken as evidence for an “anomalous metal” regime; see [31] for a review. In our view, this anomalous metal behavior is controversial; in some systems, it represents a real physical process [17] but in the others, it is an artefact caused by insufficient noise filtering [32].

Let us now consider the transitional regime between the superconducting and metallic states. The phenomenological finite-size scaling theory [4] explains how the presence of a QPT at zero temperature affects the response of a system at finite temperatures. Near a magnetic-field-driven QPT, the spatial correlation

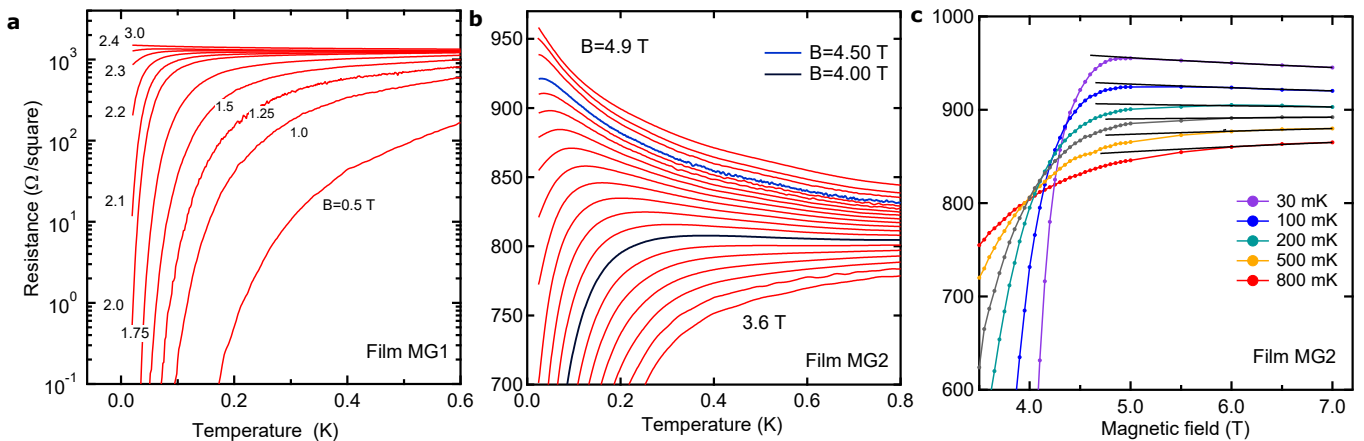


FIG. 1. **Effect of magnetic field on superconducting MoGe films.** (a,b) Resistance versus temperature for film MG1 and MG2. (c) Resistance versus magnetic field for MG2 film. The black solid lines are the linear fits to the data in the range 6-7 T extended to lower fields. They were used to estimate conductance of normal electrons.

length of the quantum fluctuations, ξ , diverges as $\xi \propto |B - B_c|^{-\nu}$, where B_c is its critical field, and ν the correlation length critical exponent. The dynamics of the fluctuations is characterized by a temporal scale ξ_τ , related to ξ as $\xi_\tau \propto \xi^z$, where z is the dynamical critical exponent. The temperature cuts off the quantum fluctuation time scale and sets in the system the dephasing length $L_\varphi \sim T^{-1/z}$. The relation $L_\varphi \lesssim \xi$ defines the boundary of the so-called quantum critical regime, where the low-bias conductivity follows the equation:

$$\sigma(B, T) = \frac{e^2}{h} L_\varphi^{-(d-2)} \Phi_\sigma \left(\frac{B - B_c}{T^{1/z\nu}} \right). \quad (1)$$

Here d is dimensionality of the system and Φ_σ is the scaling function. The limitation of the finite-size scaling theory is that it provides neither the functional form of Φ_σ nor its exact argument.

In Figure 1(b), we plot resistance of film MG2 (composition Mo₇₈Ge₂₂, nominal thickness 2.5 nm, $T_c=2.8$ K), versus temperature across the transition; the data are replotted in Fig.1(c) as a function of magnetic field. According to Eq. 1, for a 2d system ($d=2$), the prefactor is a constant and at $B=B_c$, the conductivity is independent of temperature. Experimentally, this means that there must be a temperature-independent separatrix between the superconducting-like and insulating-like $R(T)$ curves in Fig.1b and a single-point crossing for the $R(B)$ curves in Fig.1c. Neither behavior is, in fact, observed. The problem is rooted in the assumption that *all* film resistance comes from superconducting fluctuations. This assumption is natural for a “phase-only” QPT and can be valid for Josephson junction arrays but is questionable for superconducting films.

An alternative pair-breaking mechanism of QPTs requires that the density of Cooper pairs goes to zero at B_c . Moreover, close to B_c , the superconductivity becomes gapless. Both processes lead to an abundance of normal electrons contributing to the conductivity. In

our analysis, which implies the pair-breaking mechanism from the start, we adopt the two-fluid model and assume that the conductivity of the film, σ_{exp} , comes both from the normal, σ_n , and superconducting, σ_{sc} , channels. The estimate of σ_n was obtained from a linear extrapolation of $R(B)$ curves from high to low fields as shown by the solid lines in Fig. 1(c). The conductivity of the superconducting subsystem was then obtained by the simple subtraction, $\sigma_{sc} = \sigma_{exp} - \sigma_n$. The same procedure was applied to TaN and Pb films; as an example, the analysis of the latter system is presented in details in SM.

We have also added to the analysis the magnetoresistance data obtained for a single crystal of La_{1.92}Sr_{0.08}CuO₄ measured in a pulsed magnetic field up to 61 T [30]. LSCO has a layered quasi-2d structure; in the first approximation, it can be considered as a system of semi-isolated two-dimensional superconducting CuO₂ planes. The original magnetoresistance data (Fig.1 in [30]) closely resemble the data for MG2 film shown in Fig.1c. For LSCO, the normal channel conductivity σ_n was estimated from linear extrapolation of $R(B)$ curves between $B=55$ and 61 T. The data at 4.2 K appeared as an outlier in these fields and have not been included in the analysis.

The conductivity of the superconducting channel of the MG2 film, σ_{sc} , is plotted versus temperature in Fig. 2(a). The striking feature of the graph is a clear presence of an insulating (low) branch. The deviation from it, which appears as an upturn below about 30-50 mK, is likely an artefact of our subtraction procedures or is caused by the thermal decoupling of the electron subsystem. For TaN film, σ_{sc} is plotted against magnetic field in Fig.2(b); the data reveals the expected crossing of $\sigma_{sc}(B)$ curves. A similar crossing, but at a much higher field, is observed in an LSCO single crystal (Fig.2c).

According to Eq. 1, in the critical regime, all conductivity data should “collapse” onto a single curve when plotted against the scaled magnetic field. The major re-

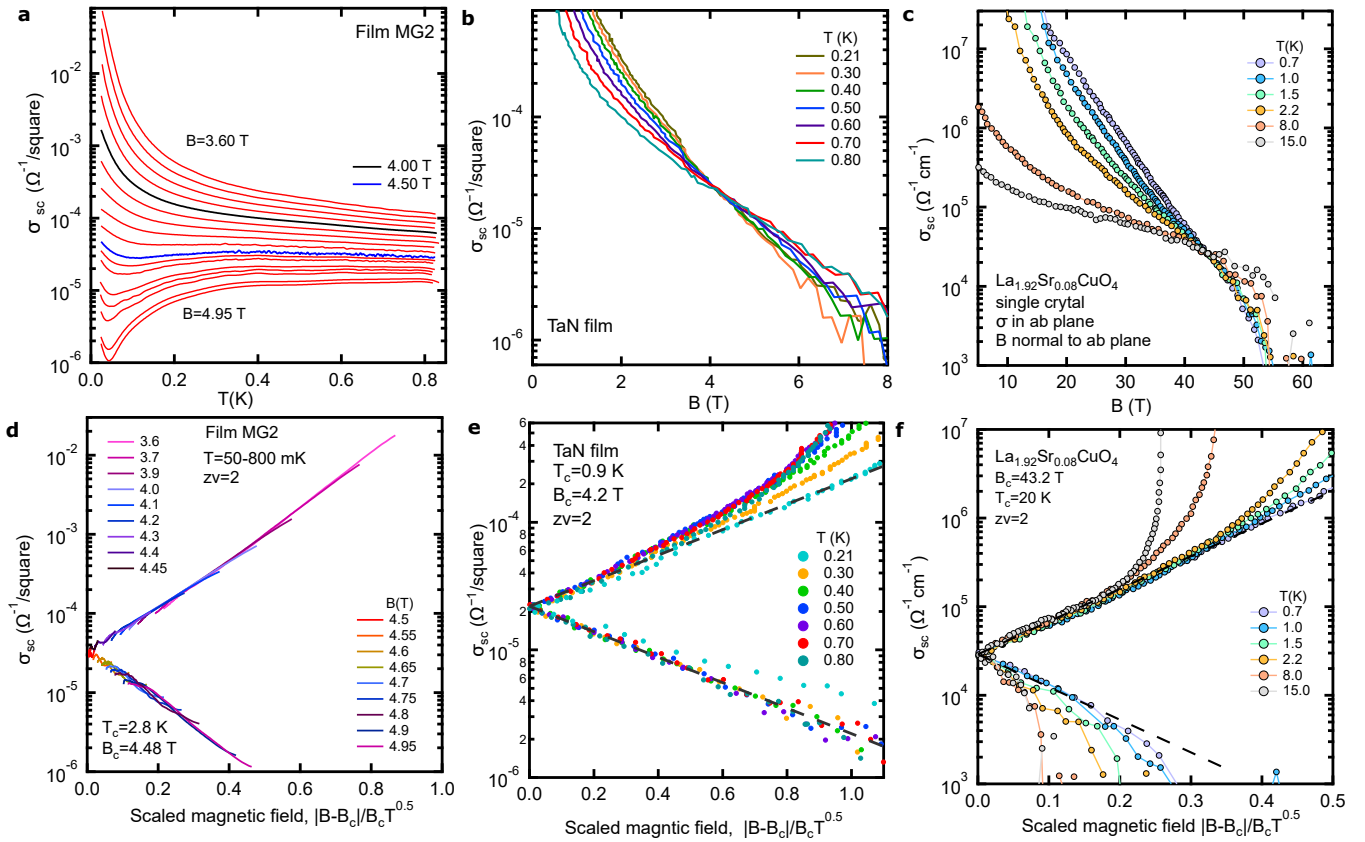


FIG. 2. **Scaling in MoGe, TaN films and LSCO single crystal.** The conductivity of superconducting channel versus temperature (a) and magnetic field (b,c) for indicated samples. (d-f) The same conductivity versus scaled magnetic field. The dashed lines in (e) and (f) indicate the exponential “mirror symmetric” variation.

sult of this work is shown in Fig.2(d-f) which displays σ_{sc} versus scaling variable $|B - B_c|/B_c T^{1/z\nu}$. A collapse of the data is obtained for the *same* value of $z\nu \approx 2$ for three MoGe, two Pb, one TaN films and surprisingly also for the LSCO single crystal. For MoGe films and LSCO, the scaling collapse occurs in an impressive temperature range exceeding one order of magnitude. Moreover, for MoGe films, where we have high-quality resistance data extended to very low temperatures, it covers 3-4 orders of magnitude of conductivity.

The data for the TaN film are also instructive. The raw $R(B)$ curves (see Fig.6 in [29]) display the crossing point and can be scaled. However, we insist that this QPT-like behavior is accidental [26]. In our view, in this and many other works, the diverging quantum correction to the normal state has been mistakenly taken as an insulating branch of the QPT.

We emphasize that σ_{sc} represents the superconducting fluctuations only. The subtraction of the dominant contribution of the normal electrons (both the Drude and quantum correction terms) is the critical step in our analysis distinguishing it from all previous work on QPTs in 2d superconducting systems.

An important question arises as to what unites the analyzed materials. We believe that this is the relatively

weak disorder and spatially uniform (in zero magnetic field) order parameter. All studied films were grown in conditions that suppress granularity and do not display so-called giant magnetoresistance peak, the known signature of a non-uniform order parameter [11, 25].

Microscopic scale of the par-breaking QPT.

The notable feature of the scaled data shown in Fig.2(d-e) is a “mirror symmetry” between the upper and lower branches. Mathematically, this means that the conductivity goes smoothly via the critical field as $\sigma_{sc} = \sigma_c \exp(-A(B - B_c)/T^{0.5})$. This dependence disagrees with perturbation theory [33] and critical theories of a pair-breaking QPT [34, 35].

In a companion papers [8, 9], we report that this exponential variation, in fact, appears in a very broad range of materials, including some magnetic and cold atom systems. Facing a question as to what characteristics of QPTs unite all these systems, we have developed a simple theoretical model based on a conjecture that the scaling theory of localization [36] describing metal-insulator transitions in 3d disordered non-interacting systems captures the general properties of a one-parameter real-space renormalization group (RG) and, in this regard, can be applied to a wide range of systems.

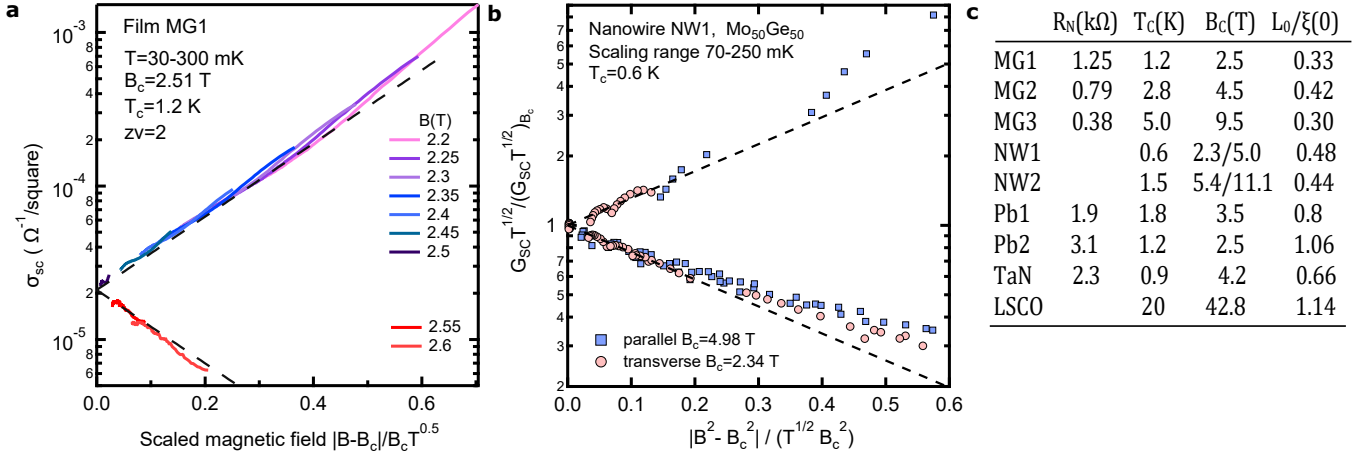


FIG. 3. **Comparison with the theoretical model of the pair-breaking QPT.** (a) Conductivity of the superconducting channel for MG1 film versus scaled magnetic field. (b) Scaled and normalized conductance of MoGe nanowire NW1 versus scaled magnetic field. Data are from [7]. In both panels, the dashed lines are the fits to the theory. (c) Experimental parameters and the extracted ratio $L_0/\xi(0)$ for indicated samples. R_N stands for normal state resistance per square. Composition for MoGe samples: Film MG1 $\text{Mo}_{50}\text{Ge}_{50}$, film MG2 $\text{Mo}_{78}\text{Ge}_{22}$, film MG3 $\text{Mo}_{78}\text{Ge}_{22}$, nanowire NW1 $\text{Mo}_{50}\text{Ge}_{50}$, nanowire NW2 $\text{Mo}_{78}\text{Ge}_{22}$. Two numbers of B_c for nanowires indicate fields in perpendicular and parallel orientations.

The exponential dependence comes from the integration of the β -function, the logarithmic derivative of the dimensionless conductance g , $\beta(g(L))=d \ln g(L)/d \ln L$, and the assumption that it varies linearly in $\ln g$ across a QPT, $\beta \approx (1/\nu) \ln g/g_c$. Here, g_c is the conductance at the critical point. Details of the derivation are given in SM and [8]. In addition to the needed exponential dependence, the model has a key parameter, L_0 , the microscopic seeding length scale from which the RG flow (integration of the β -function) starts. The generic expression of the exponential part of the scaling function in the quantum critical regime is $\exp[(L_\varphi(T)/L_0)^{1/\nu}(y-y_c)/y_c]$, where y is the driving parameter.

The adaptation of the generic model for the present case of superconducting films proceeds as follows. The theories of the pair-breaking QPT in 1d and 2d systems conclude that the dynamical exponent is $z=2$ [6, 34, 35]. With the value $z\nu \approx 2$ found from the scaling analysis, the correlation length exponent is $\nu \approx 1$. Since the microscopic pair-breaking processes in nanowires and films are similar, we use the expression for the dephasing length $L_\varphi \approx (\hbar D/k_B T)^{1/z}$ with $z=2$ as given by the critical pair-breaking theory for nanowires [6]. In this theory, the normal state diffusion coefficient, D , comes from the Cooper pair propagator for a disordered superconducting system. We can also connect L_φ with the length over which Cooper pair *density* leaks into a normal metal in the proximity effect and with the general picture of QPTs in *interacting* systems [8], according to which L_φ gives the spread of a quantum fluctuation over the Planckian time, $\tau_P=\hbar/k_B T$. For the pair-braking QPT, the relevant quantum fluctuations are the Aslamazov-Larkin-type superconducting fluctuations.

Using relation $D=v_F l/3$, where v_F is the Fermi velocity and l is the mean-free path, and the standard

BSC relations between the superconducting gap, Δ , critical temperature, T_c , Pippard coherence length, ξ_0 , and Ginzburg-Landau coherence length, $\xi(0)$, namely that $\xi_0=\hbar v_F/\pi \Delta$, $\Delta=1.76 k_B T_c$, and $\xi(0)=0.85(\xi_0 l)^{1/2}$, we obtain the following scaling equation (more details in SM):

$$\sigma_{sc} = \frac{e^2 g_c}{\hbar} \left(\frac{\hbar D}{k_B T} \right)^{-\frac{d-2}{2}} \exp \left[-1.6 \frac{\xi(0)}{L_0} T_c^{1/2} \frac{B^n - B_c^n}{B_c^n T^{1/2}} \right]. \quad (2)$$

The parameter n comes from the dependence of the pair-breaking strength on magnetic field; $n=1$ for films in a perpendicular field and $n=2$ for nanowires, the data for which have been taken from our recent work [7] and included in the analysis. The not-well-known parameters of D , v_F , and l are replaced by the experimental zero-field T_c and the ratio $L_0/\xi(0)$. A slightly different numerical factor in the exponent was used for Pb films, which comes from the relation $\Delta \approx 2.25 k_B T_c$ found in [10], and for LSCO, where the relation for a d -wave superconductor, $\Delta_{max} \approx 2.14 k_B T_c$, was used. For these two systems, we find it appropriate to use the 2d expression $D=v_F l/2$.

The derived scaling equation provides a significant step forward compared to the standard Eq.1. Both the scaling function and its argument are now well-defined. This allows extracting the seeding scale (in the present case, in the form $L_0/\xi(0)$) and testing the assumptions of the model. Figure 2(e,f) and Fig. 3 present the comparison with the experiment. Let's first notice that, as is required by Eq.2, we use conductivity per square for films (Fig. 3(a)) and conductivity multiplied by $T^{1/2}$ for nanowires (Fig. 3(b)). The dashed lines, which have the same absolute slope for the upper and lower branches, represent the best exponential fit to the data in the proximity of the critical field. From the slope of the data, the ratio $L_0/\xi(0)$ has been obtained.

The table in Fig.3(c) lists the parameters of the studied systems and presents the experimental $L_0/\xi(0)$ ratio. This is the second major result of this work. The ratio is in the range 0.66-1.14 for amorphous Pb and TaN films and LSCO and in the range 0.3-0.55 for MoGe films and nanowires.

The coherence length $\xi(0)$ represents the size of a Cooper pair. For the pair-breaking QPT where the order parameter starts to grow from zero at B_c , $\xi(0)$ is the minimal spatial scale over which superconductivity can exist and, hence, is a natural seeding microscopic length scale. Our analysis indicates that, in agreement with this physical expectation, L_0 and $\xi(0)$ match each quite well with some variation between different materials. Quantitative agreement between the scales of QPTs in MoGe nanowires and films gives strong indication that the microscopic mechanism of the transition in both systems is the same and signals a universal character of the model.

Discussion and conclusions.

The novel analysis of QPTs, which we initially developed for superconducting films, has been extended to many other systems; the results are summarized in two companion papers [8, 9]. We found that the experimental L_0 consistently matches a physically expected seeding scale, namely, it is close to (a) the mean free path for the metal-insulator transition in doped semiconductors, (b) the distance between neighboring spins in materials with Ising and Heisenberg spin chains, (c) period of the optical lattice in cold atom systems, (d) period of moiré superlattice in twisted dichalcogenide bilayers, and (e) magnetic length in quantum Hall systems. These findings validate the method and strengthen our conclusions regarding homogeneous superconducting films.

The analysis leads us to conclusion that the QPTs in the studied films occur via the pair-breaking mechanism. The evidence for this is as follows. First, the transition takes place in the background of normal electrons which contributes 0.9-0.95 of conductivity at the critical point. Secondly, the determined dynamical exponent $z=2$ is a signature of a pair-breaking QPT [6, 34, 35]. Finally, there is overall excellent consistency with QPTs in nanowires where critical pair-breaking microscopic theory is available and matches well the data.

We can further conclude that the magnetic-field-driven QPT in $\text{La}_{1.92}\text{Sr}_{0.08}\text{CuO}_4$ also occur via the pair-breaking mechanism. Hopefully this finding will help to clarify the nature of the superconductivity breakdown in over-doped cuprates in zero field. It is now debated if the breakdown occurs via a ‘dirty’ d-wave BSC pair-breaking mechanism [37] or via non-BSC mechanism [38]. The former case would be similar to our observations.

Let us notice, that in the case of the pair-breaking QPT, the exponential curves observed above the critical field do not indicate an insulating phase. Instead, they represent the conductance of the superconducting fluctuations which decreases exponentially with increasing system size.

The theoretical phenomenological analysis based on Eq.2 is not a substitute for the critical microscopic pair-breaking theory. For films, such a theory has not yet been created; numerical methods used to develop it for nanowires cannot be easily extended to the 2d case. There have to be both similarities and distinctions between QPTs in 1d and 2d. For nanowires, the critical theory includes a strong interaction between superconducting fluctuations mediated by the normal electrons. These processes must be present in films as well. On the other hand, the action of Lorentz force on Cooper pairs could be ignored in nanowires but not in films oriented perpendicular to the magnetic field.

The critical exponents obtained from the scaling analysis of the films present two interesting questions. The dynamical critical exponent $z=2$ puts the effective dimension of the films, $d_{eff}=d+z=4$, at the upper critical limit where mean-field QPTs, and correspondently $\nu=1/2$, are expected [39]. However, we found $\nu \approx 1$, indicating that the theoretical picture of QPTs needs to be revisited in this regard. The value $\nu \approx 1$ places the films right at the border of the Harris criterion $\nu \geq 2/d$, which is satisfied for disordered systems. This criterion is not satisfied for QPT in nanowires, where we also found $\nu=1$ [7], so the version of the critical theory suitable for clean systems was instead used. This could, perhaps, also be a component of a theory describing QPT in films.

In conclusion, we have observed a pair-breaking quantum phase transition in a series of superconducting MoGe, Pb, TaN films and in LSCO single crystal, and developed a novel theoretical analysis which allows for the extraction from experiment a QPT microscopic length scale. This approach enables understanding microscopic physics of QPTs in a broad range of complex systems.

Acknowledgements. A.R. acknowledges Université Grenoble Alpes and Institute Néel, where measurements were performed, for hospitality. The authors thank B. Sacépé for the help with the measurements and extensive feedback on the project. The authors also thank A. Del Maestro, E. Mishchenko, A. Zheludev, O. Starykh and P. Xiong for valuable comments. The research was supported by National Science Foundation under awards DMR1904221 and DMR2133014.

[1] B. Sacépé, M. Feigel’man, and T.M. Klapwijk, Quantum breakdown of superconductivity in low-dimensional materials, Nat. Phys. 16, 734 (2020).

[2] Y.-H. Lin, J. Nelson, and A.M. Goldman, Superconductivity of very thin films: The superconductor–insulator transition. Physica C, 514, 130 (2015).

- [3] V.F. Gantmakher and V.T. Dologopolov, Superconductor-insulator quantum phase transition, *Physics – Uspekhi*, 53 1-49 (2010).
- [4] S. L. Sondhi, S. M. Girvin, J. P. Carini, and D. Shahar, Continuous quantum phase transitions, *Rev. Mod. Phys.* 69, 315 (1997).
- [5] M. Tinkham, *Introduction to superconductivity*, 2nd ed. McGraw-Hill, New York (1996).
- [6] A. Del Maestro, B. Rosenow, and S. Sachdev, Theory of the pairbreaking superconductor–metal transition in nanowires. *Ann. Phys.* 324, 523 (2009).
- [7] H. Kim, F. Gay, A. Del Maestro, B. Sacépé, and A. Rogachev, Pair-breaking quantum phase transition in superconducting nanowires, *Nature Phys.*, 14, 912 (2018).
- [8] A. Rogachev, Microscopic scale of quantum phase transitions: from doped semiconductors to spin chains, cold gases and moiré superlattices. arXiv
- [9] A. Rogachev, Quantum phase transitions in quantum Hall and other topological systems: role of the Planckian time. arXiv
- [10] R.C. Dynes, A.E. White, J.M. Graybeal, and J.P. Garno, Breakdown of Eliashberg theory for two-dimensional superconductivity in the presence of disorder, *Phys. Rev. Lett.* 57, 2195 (1986).
- [11] T. I. Baturina, C. Strunk, M. R. Baklanov and A. Satta, Quantum metallicity on the high-field side of the superconductor-insulator transition, *Phys. Rev. Lett.* 98, 127003 (2007)
- [12] S. M. Hollen, G. E. Fernandes, J. M. Xu, and J. M. Valles, Jr., Collapse of the Cooper pair phase coherence length at a superconductor-to-insulator transition, *Phys. Rev. B* 87, 054512 (2013).
- [13] P. Szabó *et al*, Fermionic scenario for the destruction of superconductivity in ultrathin MoC films evidenced by STM measurements, *Phys. Rev. B* 93, 014505 (2016).
- [14] A. T. Bollinger, G. Dubuis, J. Yoon, D. Pavuna, J. Misewich, and I. Božović, Superconductor–insulator transition in $\text{La}_{2-x}\text{Sr}_x\text{CuO}_4$ at the pair quantum resistance, *Nature*, 472. 458 (2011).
- [15] A. Caviglia, S. Gariglio, N. Reyren, and D. Jaccard, Electric field control of the $\text{LaAlO}_3/\text{SrTiO}_3$ interface ground state. *Nature* 456, 624 (2008).
- [16] Y. Saito, Y. Kasahara, J. Ye, Y. Iwasa, and T. Nojima, Metallic ground state in an ion-gated two-dimensional superconductor, *Science* 350, 409 (2015).
- [17] C.G.L. Böttcher, F. Nichele, M. Kjaergaard, H. J. Suominen, J. Shabani, C. J. Palmstrøm, and C. M. Marcus, Superconducting, insulating and anomalous metallic regimes in a gated two-dimensional semiconductor–superconductor array, *Nature Phys.* 14, 1138 (2018).
- [18] Y. Cao, V. Fatemi, S. Fang, K. Watanabe, T. Taniguchi, E. Kaxiras, and P. Jarillo-Herrero, Unconventional superconductivity in magic-angle graphene superlattices, *Nature* 556, 43 (2018).
- [19] M. Chand *et al*, Phase diagram of the strongly disordered s-wave superconductor NbN close to the metal-insulator transition, *Phys. Rev. B* 85, 014508 (2012).
- [20] C. Carbillet *et al*, Spectroscopic evidence for strong correlations between local superconducting gap and local Altshuler-Aronov density of states suppression in ultrathin NbN films, *Phys. Rev. B* 102, 024504 (2020).
- [21] K. Bouadim, Y.L. Loh, M. Randeria and N. Trivedi, Single- and two-particle energy gaps across the disorder-driven superconductor–insulator transition, *Nature Physics* 7, 884 (2011).
- [22] A.H. Hebard and M.A. Paalanen, Magnetic-field-tuned superconductor-insulator transition in two-dimensional films, *Phys. Rev. Lett.* 65, 927 (1990).
- [23] A. Yazdani and A. Kapitulnik, Superconductor-insulator transition in two-dimensional $a\text{-MoGe}$ thin films, *Phys. Rev. Lett.* 74, 3037 (1995).
- [24] N. Marković, C. Christiansen, and A.M. Goldman, Thickness–magnetic field phase diagram at the superconductor-insulator transition in 2D, *Phys. Rev. Lett.* 81, 5217 (1998).
- [25] M. Ovadia, D. Kalok, B. Sacépé, and D. Shahar, Duality symmetry and its breakdown in the vicinity of the superconductor–insulator transition, *Nature Phys.* 9, 418 (2013).
- [26] A. Rogachev and B. Sacépé, Deficiency of the scaling collapse as an indicator of a superconductor-insulator quantum phase transition, *Phys. Rev. B* 101, 235164 (2020).
- [27] M.P.A. Fisher, Quantum phase transition in disordered two-dimensional superconductors, *Phys. Rev. Lett.* 65, 923 (1990).
- [28] P. Xiong, A. Kumar, H.J. Gardner, and L. Yu, Superconductor-insulator transition in ultra-thin a-Pb films: disorder, magnetic-field and magnetic-impurity tuning, in *Conductor-insulator quantum phase transition*, eds: V. Dobrosavljević, N. Trivedi, and J. M. Valles, Oxford University Press, Oxford (2012)
- [29] N.P. Breznay, M. Tendulkar, L. Zhang, S.-C. Lee, and A. Kapitulnik, Superconductor to weak-insulator transition in disordered tantalum nitride films, *Phys. Rev. B* 96, 134522 (2017).
- [30] Y. Ando, G.S. Boebinger, A. Passner, T. Kimura, and K. Kishio, Logarithmic divergence of both in-plane and out-of-plane normal-state resistivities of superconducting $\text{La}_{2-x}\text{Sr}_x\text{CuO}_4$ in zero-temperature limit, *Phys. Rev. Lett.* 75, 4662 (1995).
- [31] A. Kapitulnik, S.A. Kivelson, and B. Spivak, Colloquium: Anomalous metals: Failed superconductors, *Rev. Mod. Phys.* 91, 011002 (2019).
- [32] I. Tamir *et al*, Sensitivity of the superconducting state in thin films. *Sci, Adv.* 5:eaa03826, (2019).
- [33] V.M. Galitski and A.I. Larkin, Superconducting fluctuations at low temperature, *Phys. Rev. B* 63, 174505 (2001).
- [34] D. Dalidovich and P. Phillips, Transport properties near the $z=2$ insulator-superconductor transition, *Phys. Rev. B*, 63, 224503 (2001).
- [35] R. Ramazashvili and P. Coleman, Superconducting quantum critical point, *Phys. Rev. Lett.* 79, 3752 (1997).
- [36] E. Abrahams, P.W. Anderson, D.C. Licciardello, and T.M. Ramakrishnan, Scaling theory of localization: absence of quantum diffusion in two dimensions, *Phys. Rev. Lett.* 10, 673 (1979).
- [37] T.R. Lemberger, I. Hetel, A. Tsukada, M. Naito, and M. Randeria, Superconductor-to-metal quantum phase transition in overdoped $\text{La}_{2-x}\text{Sr}_x\text{CuO}_4$, *Phys. Rev. B* 83, 140507(R) (2011).
- [38] I. Božović, X. He, j. Wu, and A.T. Bollinger, Dependence of the critical temperature in overdoped copper oxides on superfluid density, *Nature*, 536, 309 (2016).
- [39] A.J. Millis, Effect of a nonzero temperature on quantum critical points in itinerant fermion systems. *Phys. Rev. B* 48, 7183 (1993)

Supplementary materials

S1. MoGe samples fabrication and measurements.

The studied films were made of two a-MoGe alloys with composition $\text{Mo}_{78}\text{Ge}_{22}$ (bulk critical temperature, $T_c \cong 7$ K) and $\text{Mo}_{50}\text{Ge}_{50}$ ($T_c \cong 3$ K). They were deposited via DC magnetron sputtering using a shadow mask with a width of $500 \mu\text{m}$. Prior to and after the film deposition, a 3-nm-thick layer of a-Ge was deposited without breaking vacuum. Measurements were carried out in a perpendicular magnetic field in a dilution refrigerator equipped with room-temperature feedthrough filters, electrical lines made of lossy miniature stainless steel coaxial cables, low-temperature copper powder-filters, and capacitance to ground, mounted directly on the sample holder. These measures were taken to prevent exposure of the films to thermal and radiative noise.

S2. Generic scaling equation.

The scaling theory of localization was originally developed to describe the conductance in disordered systems of non-interacting electrons at $T = 0$. It introduces the dimensionless conductance, g , of a hypercube of size L^d , which is related to the conductance, G , and conductivity, σ , as $\sigma = G/L^{d-2} = (e^2/\hbar)(g/L^{d-2})$. The theory makes the conjecture that the conductance of a cube of a bigger size $b^d L^d$ is determined only by b and $g(L)$. In the continuous form, this statement is expressed by the scaling equation for the function β where $\beta(g(L)) = d \ln g(L)/d \ln L$. This function describes how the conductance changes or, in the language of the renormalization group, “flows” with increasing system size, starting from some microscopic scale, L_0 , with conductance, g_0 . This theory also makes a second conjecture that $\beta(g)$ is monotonic and continuous.

Near the critical point of the metal-insulator transition (MIT), that is, near the critical conductance g_c , β behaves approximately linearly as $\beta = s \ln g/g_c$. The coefficient, s , in this equation is equal to the inverse of the correlation exponent, ν . Using this linear approximation for β , we integrate the general scaling equation for $\beta(g(L))$ starting from some microscopic conductance, g_0 , corresponding to some microscopic length scale, L_0 . For systems that exhibit an MIT, it is assumed that $L_0 \approx \ell$, where ℓ is the mean free path. However, we keep the notation L_0 in anticipation that this scale may correspond to different quantities in different systems. We also anticipate that the resulting equation is general and applicable to some 1d and 2d systems, so we keep d as a variable. In the linear regime, the integration goes as

$$\begin{aligned} \int_{g_0}^{g(L)} \frac{d \ln g}{\beta} &\approx \nu \int_{g_0}^{g(L)} \frac{d \ln g}{\ln g/g_c} = \nu \ln \left(\frac{\ln g/g_c}{\ln g_0/g_c} \right) \\ &\approx \int_{L_0}^L d \ln L = \ln \left(\frac{L}{L_0} \right) \end{aligned} \quad (3)$$

and gives $\ln(g/g_c) = \ln(g_0/g_c)(L/L_0)^{1/\nu}$. Exponentiating both sides and converting the equation to the

conductivity of a cube with side L , we find that $\sigma = e^2 g_c \exp(\ln(g_0/g_c)(L/L_0)^{1/\nu})/(\hbar L^{d-2})$.

Then, using the expansion $\ln(g_0/g_c) \approx (g_0 - g_c)/g_c$ and an approximation that near the critical conductance, g_c , the conductance changes linearly with the driving parameter y as $(g_0 - g_c)/g_c \approx (y - y_c)/y_c$ we obtain

$$\sigma = \frac{e^2}{\hbar L^{d-2}} g_c \exp \left(\frac{y - y_c}{y_c} \left(\frac{L}{L_0} \right)^{1/\nu} \right) \quad (4)$$

Equation 4 describes the variation of the conductivity of a system as a function of its size L in the critical regime at zero temperature.

At finite temperature, thermal fluctuations break the system’s coherence, so the variation given by Eq.4 switches into the Ohmic regime at the dephasing length determined by the temperature and the dynamical exponent, z . For *interacting* systems, the dephasing length is set by the Planckian time, $\tau_P = \hbar/k_B T$, as $L_\varphi \approx (b_z \hbar/k_B T)^{1/z}$, where b_z is some constant. The general theory also states that the quantum critical regime of the QPT, which we wish to analyze, is restricted by the condition $L_\varphi < \xi$. That is why the integration is taken to $L < \xi$ and the linear variation $\beta = (1/\nu) \ln(g/g_c)$ is a good approximation for the critical regime. With these inputs final equation for conductivity in the quantum critical regime of an interacting system becomes

$$\sigma = \frac{e^2}{\hbar} \left(\frac{kT}{\hbar b_z} \right)^{(d-2)/z} g_c \exp \left(\frac{y - y_c}{y_c} \frac{1}{L_0^{1/\nu}} \left(\frac{\hbar b_z}{kT} \right)^{1/z\nu} \right) \quad (5)$$

Equation 5 describes both the insulating and metallic regime. The sign in the exponent corresponds to the case when $(y - y_c) > 0$ on the metal side of the transition.

S3. Scaling equation for superconducting films and nanowires.

We start the analysis based on the conjecture that Eq. 5 captures the general properties of real-space one-parameter renormalization group and, in this regard can be applied to many systems including superconducting films and wires. We have found that the correlation length exponent in these films is $\nu \approx 1$. The dynamic exponent is $z \approx 2$ and, like in the case of superconducting nanowires, the dephasing length is taken as $L_\varphi \approx (\hbar D/kT)^{1/2}$.

For the perpendicular magnetic field, the pair-breaking strength is proportional to B , so the driving term becomes $(y - y_c)/y_c = (B - B_c)/B_c$, for nanowires the pair-breaking strength is proportional to B^2 so we have $(y - y_c)/y_c = (B^2 - B_c^2)/B_c^2$. Finally, for superconducting homogeneous films and nanowires, the only natural choice for L_0 is zero-temperature, zero-field Ginzburg-Landau coherence length $\xi(0)$. This is also the size of a Cooper pair in a disordered superconductor. From the standard BSC equations, we have $\xi(0) = 0.85(\xi_0 \ell)^{1/2}$, where ℓ is the mean free path, $\xi_0 = \hbar v_F/\pi \Delta$ is the Pipard coherence length, v_F the Fermi velocity, and Δ the

superconducting gap related to the critical temperature as $2\Delta = 3.53kT_c$. Then, taking the diffusion coefficient as $D = v_F\ell/3$, we find that not-well-known parameters, D , v_F and ℓ , drop out and general Eq.5 can be expressed for this case as following

$$\begin{aligned}\sigma_{sc} &= \frac{e^2g_c}{\hbar} \left(\frac{kT}{\hbar b_z}\right)^{\frac{d-2}{z}} \exp\left(\frac{B_c^n - B^n}{B_c^n} \frac{1}{L_0} \frac{\xi(0)}{\xi(0)} \left(\frac{\hbar D}{kT}\right)^{0.5}\right) \\ &= \frac{e^2g_c}{\hbar} \left(\frac{kT}{\hbar b_z}\right)^{\frac{d-2}{z}} \exp\left(1.6 \frac{\xi(0)}{L_0} T^{1/2} \frac{B_c^n - B^n}{B_c^n T^{1/2}}\right)\end{aligned}\quad (6)$$

In this equation $n = 1$ stands for films in perpendicular field and $n = 2$ for nanowires.

S4. Finding the conductivity of the superconducting channel for MoGe films.

The task at hand is to find a good approximation for the conductivity of a normal channel, σ_n . In our studies of nanowires, we have found that at sufficiently high fields, their resistance becomes field independent. As such, we chose the experimental value of σ_{exp} at high field to be an approximation for σ_n . This method is not applicable for films; as one can see from Fig. 1c (main text), the magnetoresistance is not zero at high fields and, moreover, it changes sign from negative at low temperatures to positive at high temperatures.

Looking for an approximation for σ_n , we have studied a film made of non-superconducting $\text{Mo}_{30}\text{Ge}_{70}$ alloy and tried to fit its magnetoresistance using the theories of quantum corrections. This film displayed an expected logarithmic correction; however, the theory did not provide an accurate quantitative dependence for $R(T, B)$ curves.

In the end, we developed two empirical methods of extracting σ_{sc} . In method 1, we employed the formula $\sigma_{sc}(T, B) = \sigma_{exp} - \sigma_n = 1/R(T, B) - 1/R(T, B_{max})$, where for σ_n we use the inverted experimental resistance at the field that gives the maximum value of R at low temperatures; for example, from Fig.1c (main text) for film MG2, $B_{max} = 5$ T. In method 2, we extended the linear fits of the data at high fields to lower fields and obtained the approximation for normal conductance as $\sigma_n = 1/[R(T, B_0) + A(T)(B - B_0)]$; this is shown for the film MG2 as solid lines in Fig.2b (main text). For MG2, $B_0 \approx 7$ T and the coefficient $A(T)$ was obtained by fitting the data in the interval 6-7 T at several temperatures; a polynomial spline was then used to get the

intermediate values of $A(T)$. Both methods produced conductivity data with a pronounced insulating branch; in both cases scaling analysis leads to the same critical exponents. Method 1 was used in the initial stage of the project and led to the discovery of the QPT, while method 2 was found to produce more compact data on the scaling plots.

S5. Conductivity of superconducting fluctuations in amorphous quench-condensed Pb films: extraction from the experimental data and finite-size scaling analysis.

We traced the data for two amorphous Pb films published Ref. 17 of the main text. They are re-plotted in Fig. 4. The films were grown inside of a dilution refrigerator by evaporation on substrates kept at low temperatures (4.2-10 K). The resistance of the films was measured with no vacuum breaking and heating them up to higher temperatures. The reference gives the technical details. The data for the film labeled by us as Pb1 were traced from Fig. 14.12 and for film Pb2 from Fig. 14.11 of this reference. The raw resistance for sample Pb1 needed to be divided by 2 to be consistent with the rest of the samples; probably an incorrect number of squares were used to compute sheet resistance (private communication from P. Xiong).

In Fig.4s we show the resistance versus magnetic field for film Pb1. As one can notice, the magnetoresistance of the films is negative at $T = 0.22$ mK and becomes positive at higher temperatures. This is a common behavior both for MoGe and Pb films.

In our analysis, we adopt the two-fluid model and assume that in the critical regime the conductivity of the film, σ_{exp} , is a sum of contributions from the normal and superconducting channels, $\sigma_{exp} = \sigma_n + \sigma_{sc}$. To estimate σ_n , the following procedure was used. We first fit the magnetoresistance data at high fields to an equation $R(B) = R(B_0) + A(B - B_0)$, where $R(B_0)$ and A are fitting parameters. For film Pb1 we set $B_0 = 8$ T and carried out fitting in the range 6-8 T; these linear fits are shown as solid lines in Fig.4c. The dependence of two fitting coefficients on temperature is shown in Fig.5a; the red lines show interpolation between the points, from which the estimate for normal channel at any given temperature and field can be computed as $\sigma_n = 1/[R(T, B_0) + A(T)(B - B_0)]$. The conductivity of the superconducting fluctuations is then computed as $\sigma_{sc}(B, T) = \sigma_{exp}(B, T) - \sigma_n(B, T)$ and shown in Fig.5b. Figure 5c shows the scaling plot of σ_{sc} .

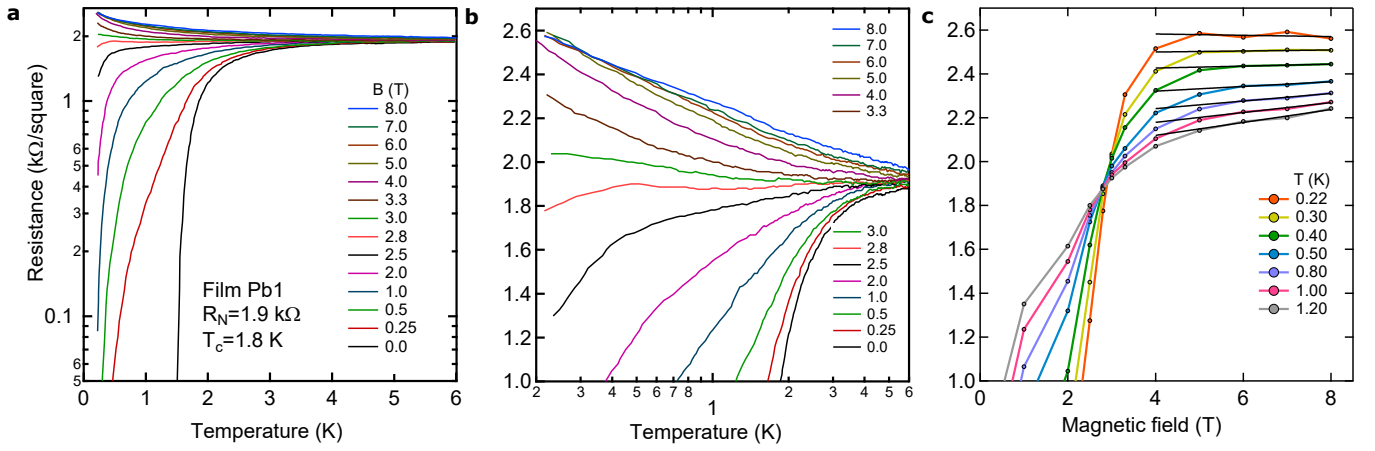


FIG. 4. (a) Resistance versus temperature for film Pb1. (b) Same data on $\log(T)$ scale to emphasize the transitional regime. The data on both panel have been traced from Fig.12 of Ref. [28] (c) Same data plotted against magnetic field. Please notice that magnetoresistance at high fields is negative at lowest temperature of the measurements. The solid lines indicate the linear fit to the $R(B)$ dependence in the range 6-8 Tesla.

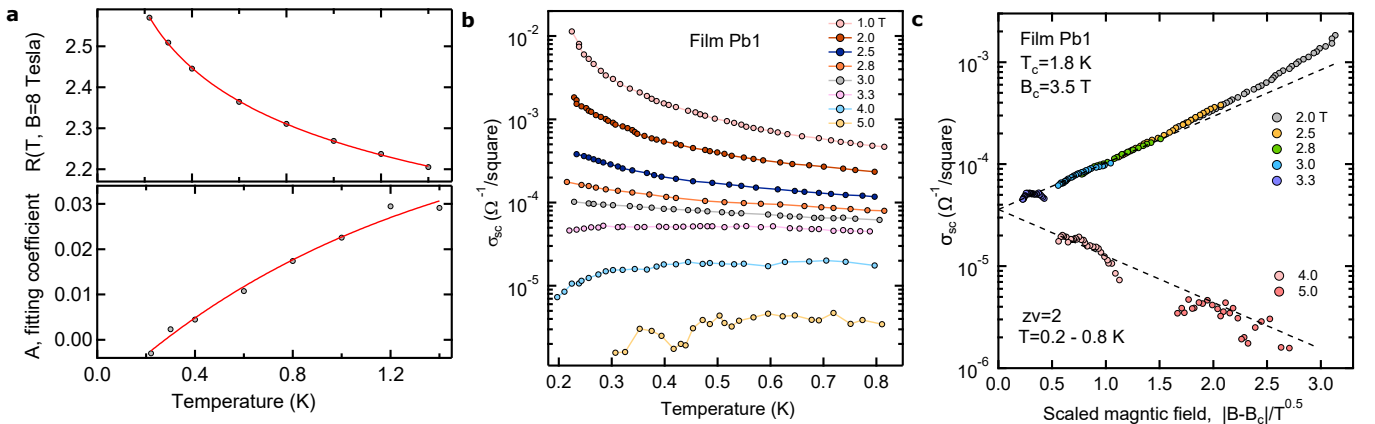


FIG. 5. (a) Interpolation of parameters $R(B_0)$ and A . (b) Conductivity of the superconducting fluctuations. (c) Scaling plot of σ_{sc} .